International Journal of Scientific Research in Engineering and Management (IJSREM)
Volume: 06 Issue: 04 | April - 2022 Impact Factor: 7.185 ISSN: 2582-3930

Transmission Line Multiple Faults Detection and Indication to Electricity Board

Kiran Jangde , Rahul Tandel , Mohammad Rizwan , Md. Rashid Ansari , Dr. Yogesh Tiwari

Abstract — In this paper, we propose a new method to locate faults on overhead power transmission lines. Line-to-ground or line-to-line faults induce transient currents in the shield wire, which flow partially to ground through the towers. In the towers closest to the fault position, the transient currents are greater and this behavior can be used to locate the fault. The method uses sensors distributed along the line, placed on the top of every tower to measure the peak currents of the transients. The sensors send these values to a computer for location processing. The method can locate faults with precision in a wide range of impedances.

Keywords — Fault location, short-circuit fault, induced voltage, induced current, shield wire, distributed sensors.

I. Introduction

There are several proposed or developed systems to locate faults on power transmission lines. The conventional systems employ methods that are very different from the proposed one. They are based on transient detection on phase cables and make the measurements only at the edges of the transmission line to estimate the fault position. These systems do not perform well with branched transmission lines because of line reflections at the branching points, and neither with parallel lines because of the mutual coupling of adjacent circuits [1].

This paper proposes a method to locate short-circuit faults on overhead power transmission lines using sensors distributed along the line, installed on the top of the towers. The fault induces transient currents in the overhead shield wire that flow partially to ground through the towers. These transient currents are greater in the towers closest to the fault position. The sensors near the fault measure these transient currents in the path to ground. Each sensor can communicate with its neighbors via embedded radio transceivers and sends the measured values to a computer using the wireless network formed by the sensor themselves. After receiving and comparing theses values, the computer can locate the fault with good precision. This method eases the installation and the maintenance of the Fault Locator System because it does not use the phase cables. It has the same precision with branched lines and parallel installations because the measurements are done close to the fault.

The method has the same principle of operation of the method used in the system of detection and location of direct lightning stroke to overhead power lines proposed in [2]. The hardware to implement both methods is the same, and they can work together complementing each other.

In the paper, we present the behavior of the induced transient currents in the shield wire and towers by simulating different types of faults in several situations to evaluate the precision of the method.

II. Voltage Induced on Shield Wire

Several papers analyze the voltage induced by the phase currents of overhead power transmission lines on metallic gas pipelines [3] and communication cables [4] running parallel to the phase cables. In a similar way, the currents in the phase cables induce a voltage on the shield wire.

Inductive coupling is the most important way to induce an AC voltage on a parallel wire. For this type of coupling, the voltage induced on a parallel wire by the current flowing in the cable is approximately equal to the product of the current by the mutual impedance between the two conductors:

$$V_m = Z_m I \quad (1)$$

where I is the current flowing in the inducing cable (Amperes), Z_m is the mutual impedance between the two parallel conductors, in ohms per kilometer, and V_m unit is given in Volts per kilometer of wire.

The voltage induced by the three phases on the shield wire of an overhead transmission line is equal to the sum of the products of each phase current by the mutual impedance between the phase cable and the wire:

$$V_m = Z_{mA} I_A + Z_{mB} I_B + Z_{mC} I_C \ (V/km) \quad (2)$$

where I_A, I_B and I_C are the currents in phases A, B, C, respectively, and Z_{mA}, Z_{mB} and Z_{mC} are the mutual impedances between phases A, B, and C and the wire, respectively. V_m is the voltage induced per kilometer of wire. The mutual impedance (Z_m) between cables above a homogenous earth can be computed by Carson's equations [5]. The equation below is a simplified version in which the corrections for earth return and cable resistance are ignored, as they represent roughly 1% of the value of Z_m[6]:

$$Z_m = \frac{\pi \mu_0 f}{4} + j\mu_0 f \left[6.5 - \ln\left(d\sqrt{\frac{f}{\rho}} \right) \right] \quad (3)$$

where f is the line frequency in Hertz, ρ is the soil resistivity in Ohm.meter, d is the distance in meters between the conductors, $j = (-1)^{1/2}$ and μ_0 is the permeability of the free space.

The mutual impedance and, consequently the induced voltage, depend on the frequency, on the distance between the cables, and on the soil resistivity. The mutual impedance increases with frequency and decreases with the distance. The frequency is the parameter that affects most the mutual impedance. The induced voltage also depends on the amplitude and balance of phase currents, and depends on the positions of the phase cables relative to the shield wire.

The current flowing in the wire between the two towers, due to the voltage induced on the wire, depends on the towers impedances, grounding resistances and the wire impedance. For the steady state currents, only the wire impedance and the towers grounding resistances are significant for the resulting current. The grounding resistance usually is higher than the wire impedance. For the high speed transient currents, the surge impedances of the wire and the towers are very significant and the wire impedance is usually greater than the tower impedance. Fig. 1 shows the equivalent circuit for the evaluation of the induced voltages and currents on shield wire and towers.

To investigate the voltages and currents induced in the shield wire by the phase currents, we used the Alternative Transient Program (ATP) [7] employing the Line/Cable routine (LCC) to model the cables. This routine calculates the inductive, capacitive and conductive coupling between the cables. There are several case studies showing that the simulation results of voltage induction using the ATP program and LCC routine is close to the field measurements [8][9].

III. Voltages and Currents Induced in Shield Wire by the Short-circuit Current

The short-circuit current in one phase induces high voltages on the shield wire because of the high frequency components of the short-circuit transient. We have used the ATP program to simulate the voltage and current induced on the shield wire

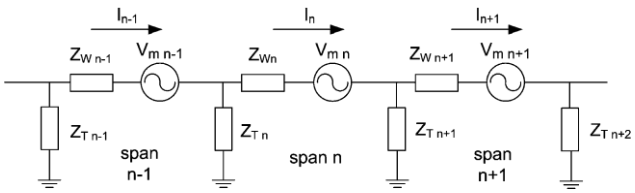

Fig. 1. The equivalent circuit for the evaluation of the induced voltages and currents on the shiel wire and towers. Z_T is the tower impedance plus the grounding resistance, Z_W is the wire impedance, V_m is the induced voltage, I_n is resulting induced current.

for a line-to-ground fault of low impedance (5 Ω) very close to a tower, in a homogeneous transmission line (detailed in Appendix A). Fig. 2 shows the short-circuit currents in one phase in the span before the fault position (source direction) and in the span after the fault position (load direction). Fig. 2 also shows the corresponding voltages induced on the shield wire.

The waveforms show that besides the 60 Hz induced voltage, there is a much higher transient voltage induced on the wire. The rise time and fall time of these short-circuit transients are very short.

The fast rate of change of the current (di/dt) shown in the figures generates frequency components much higher than 60 Hz. The knee frequency (f_{knee}) of a signal, below which most of the energy concentrates, is inversely proportional to the signal rise time (t_r) [10]:

$$f_{knee} \cong \frac{0.5}{t_r} \quad (4)$$

For the rise time of 2 μs, measured in the simulations, the short-circuit current has a knee frequency of 250 kHz. Because the mutual impedance increases with frequency, the transient voltage induced on the shield wire is much higher than the voltage induced by the 60 Hz current.

We analyzed the currents in the shield wire and in the towers closest to the position of the line-to-ground fault that generated the currents and voltages of Fig. 2. Fig. 3 shows the diagram of the segment of the transmission line near the fault and the currents simulated. The six towers where the currents were measured have the identifications T1 to T6 in the figure.

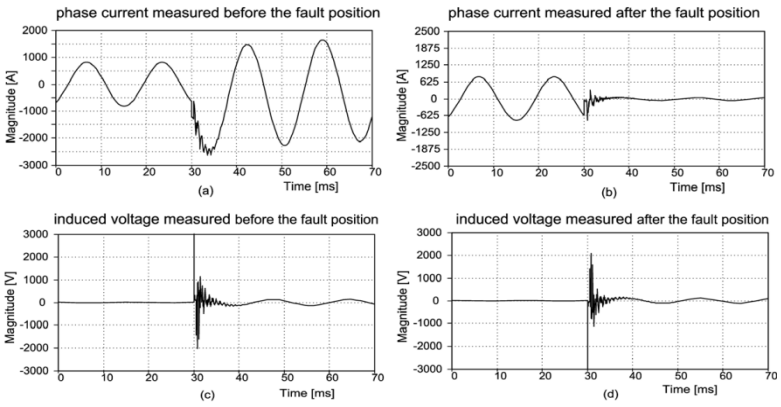

Fig. 2. Line-to-ground fault currents before (a) and after (b) the short-circuit position; Voltage induced on the shield wire before (c) and after (d) the short-circuit position.

The fault is very close to T4. Fig. 4 shows the waveform of the transient currents in the shield wire in the six towers near the fault position, according to Fig. 3. The figure shows that the tower closest to the short-circuit position is the one with the highest current (tower 4) and the highest rate of change of current (di/dt). In the other towers, the transient currents that flow through the towers are smaller and have lower di/dt (towers 1, 2, 3, 5 and 6). The currents in the shield wire connected to these five towers have similar amplitude and waveform and cancel each other when they flow to ground through the tower. This behavior is the same in all spans that are not near the fault. Besides, between these five towers, the two towers closest to the short-circuit position have the highest transient currents (towers 3 and 5) because the currents in their segments of shield wire are less similar and the cancellation is smaller. In tower 4, the currents in the two adjacent spans are quite different and the resulting current in the tower is much higher.

In the simulations of line-to-ground faults in the middle of the span, and other intermediary positions, we observed the same behavior. In the two towers closest to the short-circuit position, the induced transient currents are higher and have a higher di/dt. In the other towers, the currents and their di/dt are lower. Other simulations showed the same behaviour with other types of symmetrical and asymmetrical faults like phase-to-phase short-circuits.

IV. USING THE TRANSIENT CURRENTS INDUCED BY THE SHORT-CIRCUIT TO LOCATE THE FAULT

We made several simulations changing the parameters of the line and of the faults and verified that the transient currents induced by the short-circuit fault always have amplitude and rate of change of current (di/dt) higher in the towers near the fault location. This characteristic allows the detection and location of the fault by measuring the transient induced currents flowing in the towers and comparing the measured values. The towers with the higher transient currents (or di/dt) are the ones closest to the fault position.

A straightforward way to measure the transient current flowing to ground through the tower is to use a Rogowski coil [11] placed on the top of the tower, around the tip of the structure where the wire is connected, or around the wire connecting the shield wire to the tower structure (Fig. 5). The output voltage of the Rogowski coil is proportional to the rate of change of the current flowing through the toroid. It has good transient response and operates on a wide range of currents. Applying this voltage to an integrator circuit results in an output voltage proportional to the current flowing to ground (through the toroid). The integrator is usually placed close to the coil to minimize noise pickup. To integrate only the higher frequency transient current, the integrator can be implemented by a low-pass filter with corner frequency much higher than 60 Hz. The 60 Hz component of the steady state

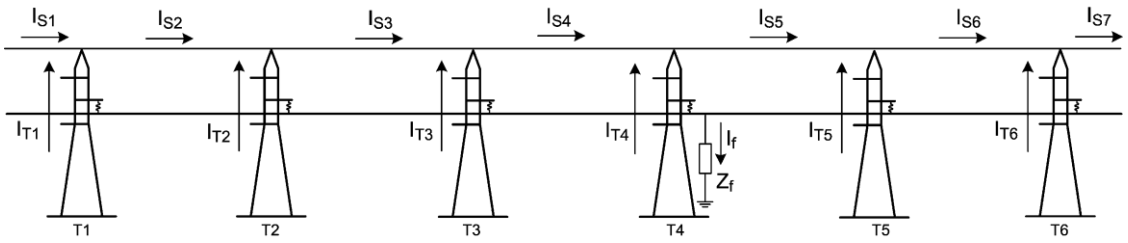

Fig. 3. Currents in the shield wire and in the towers near the fault position, I_{S1} to I_{S7} are the shield wire currents, I_{T1} to I_{T6} are the tower currents, Z_f is the short-circuit impedance, I_f is the short-circuit current (T1 to T6 are the identifications for tower 1 to tower 6).

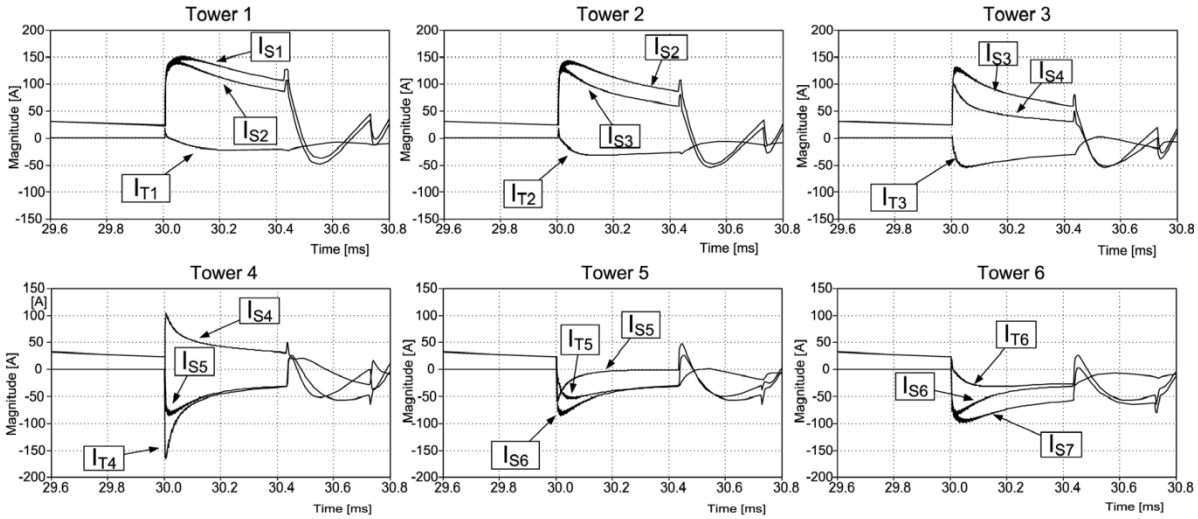

Fig. 4. Waveforms of the transient currents in the shield wire and towers according to Fig. 3.

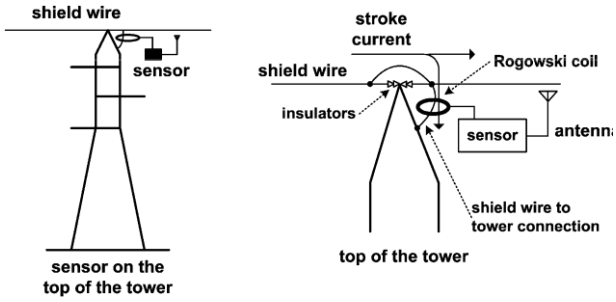

Fig. 5. Position of the sensor on the top of the tower.

current is filtered out in the process of integration. The integration also eliminates undesired noise with frequency much higher than the frequency of fault transients. In Appendix B, we detail the operation and characteristics of the Rogowski coil and integrator.

An electronic intelligent sensor, placed on the top of each tower, must be triggered to read the output voltage of the integrator whenever this voltage reaches a preset threshold. The output is much higher for the transient induced current than for the steady state induced current. The sensor detects the peak value of the voltage, converts the analog measurement into binary data and sends it to a computer for processing. The sensors that measure the greatest values of the current are the ones closest to the fault. Less than a dozen sensors at each side of the fault will measure a significant value. Together with the peak value, each sensor must send the tower identification number. Installing one sensor at each tower allows for the detection and location of the fault.

The method is also applicable to DC power transmission lines. In this case, there is no AC steady state induced current, there is only the transient current induced in the shield wire.

V. SHORT-CIRCUIT SIMULATIONS TO EVALUATE THE PRECISION OF THE FAULT LOCATION METHOD

To evaluate the precision of the method, we made several simulations using the ATP program to analyze the behavior of the transient induced currents in different situations. We simulated different types of short-circuits in homogeneous and non-homogeneous, transposed and untransposed overhead power lines. We tested short-circuit faults in different positions, changing characteristics like the length of the line, span lengths, tower height, tower impedance, tower grounding resistances and soil resistivity. We simulated short-circuits of one, two and three phases to ground, short-circuits between phases, and both low impedance and high impedance faults. The value of the currents and the instant of the faults (related to the waveform cycle) were also changed.

Table I and Table II show the results for two sets of these simulations for a non-homogeneous transmission line. In Appendix A, we detail the characteristics of the line and the simulation. The measurement of the currents included 19 towers but only the eight towers closest to the fault are shown to reduce the tables. In the tables, the towers are identified as T1 to T8. In Table I the faults occur in T4 (or very close to it). In Table II the faults occur in the middle of the span between T4 and T5. Table I and Table II include line-to-ground faults and line-to-line faults. Table I also includes short-circuits from phase to the tower structure at 21 m from the bottom of the tower (position of the lower cables). The results show the absolute peak values (Volts) measured by the Rogowski coil and integrated by a low-pass first-order active filter with corner frequency of 1500 Hz (details in Appendix B).

Table I shows that the peak value of the transient current is much higher in the tower closest to the fault (T4) than in the other towers (bold values). Table II shows that the peak values in T4 and T5 have close values, which are much higher (bold values) that in the other towers. Despite the variation of the tower grounding resistances and the variation of the length of the spans, the towers closest to the fault have the highest transient currents.

Analyzing the several simulation results, there are some situations that generate a small value of transient current and consequently a small value of di/dt: high impedance short-circuits; one-phase-to-ground faults that occur when the voltage of the short-circuited phase is close to zero; and phase-to-phase faults when the voltage of the two shorted phases are close. Despite the measurement flexibility of the

TABLE I
RESULTS OF THE FAULT SIMULATIONS IN T4

fault type	fault	integrator output (Volts)							
	Resist.	T1	T2	T3	T4	T5	T6	T7	T8
phase A to ground	5 Ω	5.3	10.4	14.3	**44.5**	17.1	5.8	6	2.9
phase A to ground	50 Ω	4.6	8.6	11.0	**36.5**	12.2	4	5.3	2.4
phase A to ground	1 kΩ	1.3	1.8	2.5	**8.3**	2.5	1.0	1.5	0.7
phase A to ground	10 kΩ	0.2	0.2	0.3	**1.0**	0.3	0.1	0.2	0.1
phases A and B to ground	50 Ω	5.4	9.8	12.9	**42.9**	14.1	4.6	6.3	2.8
phase B to tower	1.5 Ω	2.8	5.3	6.6	**32.9**	7.4	3.6	2.9	1.3
between phases A-B	2 Ω	1.8	2.4	3.4	**11.3**	4.2	2.2	1.8	0.9

TABLE II
RESULTS OF THE FAULT SIMULATIONS IN THE MIDDLE OF THE SPAN (BETWEEN T4 AND T5)

fault type	fault	integrator output (Volts)							
	Resist.	T1	T2	T3	T4	T5	T6	T7	T8
phase A to ground	5 Ω	4.6	7.8	8.1	**34.7**	**39.6**	8.5	5.6	3.1
phase A to ground	50 Ω	4.2	5.7	6.7	**30.1**	**33.7**	6.5	5.1	2.6
phase A to ground	1 kΩ	1.1	1.2	1.9	**7.7**	**8.3**	1.5	1.6	0.7
phase A to ground	10 kΩ	0.2	0.2	0.3	**0.9**	**1.0**	0.2	0.2	0.1
phases A and B to ground	50 Ω	4.8	6.8	7.7	**34.7**	**39.0**	7.4	5.9	3.0
between phases A-B	2 Ω	1.7	2.3	3.5	**11.4**	**12.2**	3.8	2.7	1.2

Rogowski coil, the wide range of values can be a problem to the integrator circuit. To get around this problem, each sensor may have two or more coils placed around the wire to work with a lower range of values: one for detection of high values and another one for detection of lower values.

The simulated power lines have one shield wire but the results are fully applicable to lines with two shield wires, measuring the currents from only one in each tower. The second shield wire has the effect of reducing the attenuation of the transient currents in the adjacent towers but the simulations showed the same behaviour of the currents with the highest peak values on the towers closest to the fault.

VI. Detection and Location System and Fault Location Processing

The system to detect and locate the faults must have the following components: the Rogowski coils to measure the currents; sensors to read the measured currents and send the values to the computer; a communication structure to send the data from the sensors to the computer for processing; and a computer to process the values sent by the sensors. Batteries recharged by small solar cells may supply the power to the sensors. Another option is to use the 60 Hz steady state current induced in the shield wire. A current transformer installed around the shield wire can supply AC power to the sensor and to charge the batteries [12].

When there is a transient current in the tower, if the output of the integrator exceeds a preset threshold (to avoid reading very small transients from other sources), the sensor reads this output voltage and sends the peak value and the tower identification to the computer, through the communication subsystem. The computer processes the information received from the sensors and locates the fault.

The location process is straightforward. After receiving the values sent by the sensors, together with the tower identification, the computer locates the two highest peak values and the corresponding tower identification. The fault position is located between these two towers. If one of the two sensors measured a peak value much higher than the other one, 100% or more, there is a high probability of a short-circuit in the tower (or very close to it) with the highest transient current.

To transmit the information to the computer, each sensor has to communicate through its radio frequency transceiver. The power transmission line may have the extension of hundreds of kilometers. It is not feasible to have direct radio communication between each sensor and the computer. The radio transceiver in every sensor may be a Zigbee transceiver [13] to convert the set of sensors into a wireless Zigbee network. Therefore, the sensors can send the data to the computer through the network of sensors. In this case, each sensor retransmits the data to its neighbor until it reaches the end of the line, where the computer receives the data. 900 MHz ZigBee transceivers with 10 dBm power output, operating at 20 kbps with -110 dBm sensitivity, have an outdoor line-of-sight range of up to 6 km with a 3 dBi antenna [14]. This range allows each sensor to communicate with several neighbors sensors giving the necessary redundancy in case of a failure of some consecutive sensors.

VII. Conclusions

The proposed method allows a great precision in the location of faults. It is possible to determine the tower or the span where the fault has occurred. It allows the location of faults in a wide range of impedances. Besides, it is possible to apply the method on both AC and DC transmission lines**.** The method is fully applicable to branched transmission lines or parallel transmission lines.

Despite the high number of sensors necessary in a typical transmission line with the length of hundreds of kilometers (hundreds of sensors), the cost of a system implementing the proposed method is very low compared to the power transmission line itself and the benefits of minimizing outage time. The high number of sensors also decreases the cost of each sensor. One such system is simple and accurate and can be very reliable with proper product engineering. Besides, the installation is easy and the sensors could even been installed with the line in operation because the phase cables are not used for measurement.

Acknowledgment

The authors would like to thank FAPEMIG (Fundação de Amparo à Pesquisa do Estado de Minas Gerais) and CDTN (Centro de Desenvolvimento da Tecnologia Nuclear) for their financial support.

References

[1] IEEE Power Engineering Society, “IEEE Guide for Determining Fault Location on AC Transmission and Distribution Lines,” june 2005.
[2] D. T. Silva, J. L. Silvino, J. C. D. de Melo, “Detection and location of direct lightning strokes to overhead power transmission lines by measuring currents from shield wires,” unpublished (accepted for presentation at the 9th IEEE/IAS International Conference on Industry Applications).
[3] Akihiro Ametani, Yuji Hosakawa; “EMTP simulations and theoretical formulation of induced voltages to pipelines from power lines”; IPST Conference 2007; Lyon, France.
[4] J. O. S. Paulino, “Influence of Short-Circuits on Distribution Networks over the Phone Networks Using Mutual Posts,” Marter’s Degree Dissertation, Electrical Engineering Department, Federal University of Minas Gerais, December 1987, in portuguese.
[5] H. W. Dommel, “Electromagnetic and electrostatic effects of transmission lines practical problems, safeguards and methods of calculation,” IEEE Transactions on Power Apparatus and Systems, Volume PAS-93, Issue 3, May 1974, pp:892 – 904.
[6] G. M. Amer, “Novel technique to calculate the effect of electromagnetic field of HVTL on the metallic pipelines by using EMTP program,” COMPEL: The International Journal for Computation and Mathematics in Electrical and Electronic Engineering 2007 Vol. 26 Issue 1.
[7] “Alternative Transients Program (ATP) - Rule Book,” Canadian/ American EMTP User Group (1987-1998).
[8] C. Chunkull, K. Tunlasakun, S. Nomnamsapl and N. Chayawattol, “A study of the mutual coupling between a three-phase power line 115 kV and a parallel telephone line by using ATP/EMTP: case study distribution line in thailand alarm,” SICE-ICASE International Joint Conference 2006 Oct. 18-2 1, 2006 in Bexco, Busan, Korea.
[9] H. W. Dommel, “Electromagnetic Transients Program - Theory Book,” BPA Portland, USA, August 1986.
[10] H. Johnson and M. Graham, “High Speed Digital Design: A Handbook of Black Magic,” Prentice-Hall, Upper Saddle River, NJ (1993).
[11] J. F. Arcega, J. A. Artero, “Current sensor based on rogowski coil,”

ICREPQ 2004 - International Conference On Renewable Energies And Power Quality (March 2004), Barcelona, Spain.
[12] D. T. Silva, J. L. Silvino, J. C. D. de Melo, "Power harvesting from shield wire for monitoring apparatus on overhead transmission lines," unpublished (accepted for presentation at the 9th IEEE/IAS International Conference on Industry Applications).
[13] ZigBee Alliance, "ZigBee Specification v1.0," April 14, 2005.
[14] Meshnetics, "ZigBit 900 OEM Modules - Ultra-Compact 868MHz/915MHz IEEE 802.15.4/ZigBee Modules for Wireless Networking Applications," Product Datasheet, March 2008.
[15] "Estimating Lightning Performance of Transmission Lines II Updates to Analytical Models," IEEE Working Group Report, 92 SM 453-1 PWRD.
[16] W. A. Chisholm, Y. L. Chow and K. D. Srivastava, "Travel time of transmission towers," IEEE Transactions on Power Apparatus and Systems (1985), PAS-104, (10), pp. 2292-2928.
[17] L. Prikler, H. K. Høidalen, "ATPDraw version 3.5 for Windows 9x/NT/2000/XP User's Manual," Aug. 2002.

APPENDIX A

Fig. A1 shows the dimensions of the tower modelled in the simulations and the position of each cable. Each tower is represented as a transmission line with surge impedance of 155 Ω, calculated using the method recommended by IEEE [15] and the propagation velocity in the towers is 2.5 x 10^8 m/s [16]. The phase cables and ground wires are modeled by the Line/Cable objects (LCC) of ATPDraw program [17] and the soil resistivity is 500 Ω.m, which a reasonable value for the high resistivity soil in Brazil. The impedances of the supply network, including the short-circuit reactance of the transformer bank, are included in the simulations.

The simulatated homogeneous power transmission line have 11 towers spaced 500 m apart (5 km transmission line) plus a 50 km LCC section at each end as line terminations (total length of 105 km). The tower grounding resistances are 20 Ω. The fault is simulated at 52.5 km from the source.

The simulated non-homogeneous power transmission line have 19 towers (5 km transmission line) plus a 50 km LCC section at each end as line terminations (total length of 105 km). Most of the span lengths are 300 m but the spans lengths between the 10th and 15th towers are 100 m, 300 m, 200 m, 400 m and 100 m, respectively. The tower grounding resistance for most of the towers is 20 Ω, except the resistances of 10th and 12th towers with 40 Ω and 10 Ω, respectively. The faults are simulated at 54 km from the source between the 10th and 11th towers.

All faults occur 6 ms after the beginning of a voltage cycle of phase A and the current in each phase is 600 A_{rms}.

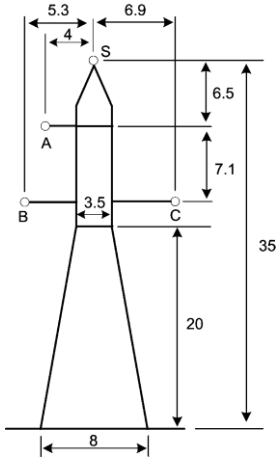

Fig. A1. Tower dimensions (m) and the positions of the phase cables (A, B, and C) and the shield wire (S) (m).

APPENDIX B

The Rogowski coil is a coil with turns equally distributed along a non-magnetic core. The return wire goes back concentrically to avoid the external fields produced by external currents near the coil (Fig. A2). The placement of the coil is very easy due to the construction of the coil in an open ring shape that closes mechanically around the conductor where the current to be measured is flowing.

The Rogowski coil voltage *v(t)* is proportional to the rate of change of the current by the constant *K*, which depends on the construction characteristics of the coil:

$$v(t) = K\frac{di}{dt} = -\mu_0 \frac{N}{l} A \frac{di}{dt} \qquad (5)$$

where μ_0 is the vacuum permeability, *N* is the number of turns, *l* is the mean length of the toroid and *A* is the area of the turn. Integrating the voltage *v(t)*, we obtain an output voltage, $v_{out}(t)$, proportional to the original current *i(t)* by the time constant *RC* of the integrator:

$$v_{out}(t) = \frac{1}{RC}\int v(t)dt = \frac{1}{RC}\mu_0 \frac{N}{l} Ai(t). \qquad (6)$$

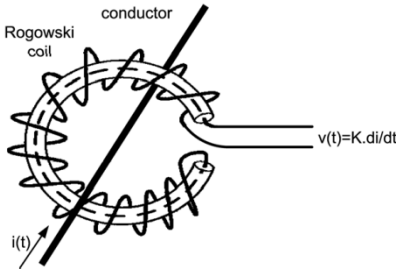

Fig. A2. Measurement of current using Rogowski coil, *i(t)* is the currentbeing measured, *v(t)* is the coil voltage, and *K* is a constant.

The most important characteristics of a Rogowski coil are large bandwidth, large range, good linearity (non-magnetic core), no saturation, easy installation, and galvanic isolation between the primary circuit and the measuring circuit.

In the simulations, the ATP equivalent circuit of the Rogowski coil is a TACS device simulating a coil with 300 turns, 7.5 cm toroid radius, 2 cm turn radius (*K* constant equal to 10^{-6}). The device includes the approximated frequency response in its transfer function. To integrate the signal, the output of the simulated coil passes through a low-pass first-order active filter with corner frequency of 1500 Hz and amplification factor equal to 20 (TACS device). The filter works as an integrator for frequencies well above 1500 Hz. The resulting integration restores most of the transient currents but attenuates the 60 Hz steady state currents and other low frequency components.